

Original article

A multi-continuum model for simulating in-situ conversion process in low-medium maturity shale oil reservoir

Zijie Wang[✉], Jun Yao*, Hai Sun[✉], Xia Yan, Yongfei Yang[✉]

School of Petroleum Engineering, China University of Petroleum (East China), Qingdao 266580, P. R. China

Keywords:

Multi-continuum model
low-medium maturity
hydro-thermal coupling
in-situ conversion
compositional model

Cited as:

Wang, Z., Yao, J., Sun, H., Yan, X., Yang, Y. A multi-continuum model for simulating in-situ conversion process in low-medium maturity shale oil reservoir. *Advances in Geo-Energy Research*, 2021, 5(4): 456-464, doi: 10.46690/ager.2021.04.10

Abstract:

In-situ conversion is proposed applicable for low-medium maturity shale oil reservoir. However, parallel chemical kinetic reactions and evolution of shale pores during in-situ conversion make the numerical simulation a challenging problem. Although shale is typical multiscale and heterogeneous media, few models in previous studies take the difference between organic and inorganic system into consideration, which cannot simulate fluid flow accurately. In this paper, a multi-continuum model, considering coupled thermal-reactive compositional flow, is developed to simulate in-situ conversion process in low-medium maturity shale oil reservoir. The reaction of kerogen and hydrocarbon is quantified using kinetic reaction model. The evolution of fluid composition and shale properties are also incorporated. The accuracy of multiple-interacting-continua model and compositional model are demonstrated by comparing with commercial software and analytical solution. Then, the typical hexagon vertical well heating pattern is simulated and the feasibility is evaluated from an economic aspect. Finally, a series of case studies are conducted to investigate the impact of operation parameters on shale oil production.

1. Introduction

Continental shale oil is widely distributed in China and is mainly of low-medium maturity (Yang et al., 2019b; Gao et al., 2020). The natural maturation of such shale resource usually takes long time (Braun and Burnham, 1987, 1990). Therefore, low thermal maturity shale is mainly surface retorted in last decades (Hazra et al., 2013). However, the ex-situ retorting can cause damage to environment and obtain low quality oil products (Fowler and Harold, 2009; Bi et al., 2020; Oja and Eric, 2020). Recently, in-situ conversion process is put forward to be feasible for clean and effective development of low-medium maturity shale oil reservoirs (Zhao et al., 2020).

During the in-situ conversion process, kerogen pyrolysis and hydrocarbon cracking are involved when formation temperature reaches the appropriate window. These kinetic reactions have great impact on fluid composition, leading to phase evolution and disappearance. And the reservoir fluid properties (e.g., viscosity, density and specific capacity) can vary a lot from initial state (Kibodeaux, 2014). Meanwhile, shale pore space increases because solid organic matter (e.g.,

kerogen) is pyrolyzed into oil and gas, improving shale porosity and permeability (Garipov et al., 2018). In conclusion, these unique phenomena during artificial maturation process make the accurate and efficient simulation of in-situ conversion process remain a challenging problem.

Shale is complex mixture of different media (Naraghi and Farzam, 2015; Yang et al., 2019a). Dual-porosity model was first proposed by Barenblatt (1960) and then developed by Warren and Root (1963), in which shale is separated into fracture and matrix. Nevertheless, the inorganic constituent has wider range of pore size distribution (from 10 nm to 100 μm) while the organic matter mainly consists of nanopores and macropores (from 10 to 500 nm) (Fan et al., 2018; Zhu et al., 2020). In addition, organic pores play an important role in retained fluid storage, and organic substance pyrolysis can provide additional hydrocarbon (Wang et al., 2015). Therefore, it is necessary to treat organic and inorganic system separately. Zhang et al. (2015) presented a novel triple-continuum model, in which different transfer model was used. However, the triple-continuum model may be inaccuracy in shale oil reser-

voirs because it usually takes long time to reach pseudo steady state (Yan et al., 2018). The multiple-interacting-continua (MINC) model is applied to describe the transient fluid transfer among multiple continuum, in which the primary matrix grid cell is divided into a series of nested subcells (Wu and Pruess, 1988; Liu et al., 2021a). And the accuracy of MINC model in unconventional reservoir is proved (Farah et al., 2014).

A number of simulation studies have been conducted on multiscale shale reservoir. Yan et al. (2018) presented an efficient hybrid model for fractured shale reservoir, in which MINC method was used to represent shale matrix and natural fractures. Cheng et al. (2020) simulated shale gas flow with multiple mechanism by using MINC and embed discrete fracture model (EDFM). Liu et al. (2020a) proposed a novel modified EDFM method for 3D unconventional reservoir with complex fractures. Jiang and Rami (2015) developed a novel model using unstructured discrete fracture model and MINC, which had better flexibility for non-ideal fracture geometry. In addition, a few simulation studies are carried out on in-situ conversion process in recent years. Fan et al. (2010) presented a thermal-compositional model, in which parallel chemical kinetic reactions were considered. However, the multiscale pore space in shale reservoir was neglected and effective porosity was used instead. Egboga et al. (2017) evaluated the thermal enhance oil recovery in shale oil reservoir from economic aspect based on CMG Stars simulator. However, only partial chemical reactions were considered and K-value based flash calculation can cause inaccuracy. Lee et al. (2016) took shale matrix and natural fractures into consideration and proposed a thermal-chemical coupled numerical model, in which MINC was used to simulate matrix and fracture interaction. Whereas, few studies divided shale matrix into inorganic and organic constituent during the simulation of in-situ conversion, which can diverge widely from actual fluid flow in shale oil reservoir.

To this end, a novel multi-continuum model considering coupled thermal-reactive flow is presented, to investigate the practicability of in-situ conversion process in low-medium maturity shale oil reservoir. In our model, first order parallel kinetic reaction model is used to quantitatively describe kerogen pyrolysis and subsequent hydrocarbon cracking. Meanwhile, MINC method is applied to handle the transient fluid transfer between inorganic and organic system. Then, based on our proposed model, typical hexagon heating pattern is simulated and evaluated from economic aspect. And sensitivity analysis is conducted on important influencing factors including heating temperature and heating pattern.

2. Numerical model and schemes

2.1 Mass and energy conservation equations

During in-situ conversion process, a series of chemical kinetic reactions are involved, which is treated as the nonlinear source term. And the mass conservation equation for each mobile component is given below:

$$\begin{cases} \frac{\partial}{\partial t} \left[\phi \sum_{\beta} (S_{\beta} \rho_{\beta} X_{i\beta}) \right] = -\nabla \cdot \sum_{\beta} (\rho_{\beta} X_{i\beta} u_{\beta}) \\ + \sum_{\beta} \rho_{\beta} X_{i\beta} q_{\beta}^w + \sum_{\beta} \sum_k (v'_{i\beta,k} - v_{i\beta,k}) r_k \\ - \nabla \cdot (\rho_w u_w) + \rho_w q_w = \frac{\partial(\phi \rho_w S_w)}{\partial t} \end{cases} \quad (1)$$

where indices i and β refer to components and phases, respectively; subscript k represents k -th reaction; ϕ is the shale porosity; molar fraction of component i in phase β is $X_{i\beta}$; ρ_{β} and ρ_w are molar density of phase β and water, mol/m³, respectively; q_{β}^w and q_w are source/sink term of phase β and water per unit volume, mol/(m³·s), respectively; $v'_{i\beta,k}$ and $v_{i\beta,k}$ represent the stoichiometric coefficients of component i in phase β in k -th reaction as product and reactant, respectively; r_k is the reaction rate of reaction k , s⁻¹; S_{β} and S_w are the fluid saturation of phase β and water, respectively; u_w is the velocity of water, m/s; u_{β} is the velocity of phase β , m/s, given by Darcy's law:

$$u_{\beta} = -\frac{K k_{r\beta}}{\mu_{\beta}} \nabla \psi_{\beta} \quad (2)$$

where K is the shale permeability, m²; $k_{r\beta}$ is relative permeability of phase β ; μ_{β} is viscosity of phase β , mPa·s; ψ_{β} represents the pseudo potential of phase β , defined as $\psi_{\beta} = p_{\beta} - \rho_{\beta} g D$, Pa; p_{β} is pressure of phase β , Pa; g is gravity constant, 9.8 m/s²; D is reference depth, m.

Solid organic component is immobile, and the mass conservation equation can be simplified as:

$$\frac{\partial C_S}{\partial t} = \sum_k (v'_{s,k} - v_{s,k}) r_k \quad (3)$$

where C_S is kerogen concentration, mol/m³; $v'_{s,k}$ and $v_{s,k}$ represent the stoichiometric coefficients of solid organic component in k -th reaction as product and reactant, respectively.

The energy conservation equation is simplified by assuming local thermal equilibrium and neglect chemical reaction enthalpy (Lee et al., 2018b; Liu et al., 2021b):

$$\begin{aligned} \frac{\partial}{\partial t} \left[\phi \left(\sum_{\beta} U_{\beta} \rho_{\beta} S_{\beta} \right) + (1 - \phi) \rho_R U_R \right] = \\ - \nabla \cdot \left(\sum_{\beta} H_{\beta} \rho_{\beta} u_{\beta} \right) + \nabla \cdot (\kappa \nabla T) + \sum_{\beta} H_{\beta} \rho_{\beta} q_{\beta}^w + q^H \end{aligned} \quad (4)$$

where index R refers to shale rock; U_{β} and U_R is the internal energy of phase β and shale rock, respectively, J/mol; ρ_R is density of shale rock, kg/m³; κ is the comprehensive thermal conductivity, given by $\kappa = (1 - \phi) \kappa_r + \phi (S_o \kappa_o + S_g \kappa_g + S_w \kappa_w)$, W/(m·K); S_o and S_g are saturation of oil and gas phase, respectively; κ_o , κ_g and κ_w are thermal conductivity of oil, gas and water phase, respectively; T is shale formation temperature, K; q^H is the energy injected through horizontal heating well per unit time per volume, J/(m³·s); H_{β} is fluid enthalpy of phase β , J/mol, given by:

$$H_{\beta} = \sum_i X_{i\beta} H_i \quad (5)$$

where H_i is the enthalpy of component i , J/mol, defined as a function of temperature:

$$H_i = H_{ai} + H_{bi}T + H_{ci}T^2 + H_{di}T^3 + H_{ei}T^4 + H_{fi}T^5 \quad (6)$$

where $H_{ai} \sim H_{fi}$ are the enthalpy coefficient of component i .

Cubic equation of state based flash calculation is used in compositional model. The phase equilibrium is reached when fugacity of each component i within different phases is equivalent:

$$f_{i\beta}(p, T, X_{i\beta}) = f_{i\gamma}(p, T, X_{i\gamma}) \quad (7)$$

where $f_{i\beta}$ is the fugacity of component i in phase β ; $X_{i\beta}$ and $X_{i\gamma}$ are the molar fraction of component i in phase β and phase γ , respectively. Sequentially, phase density, viscosity and enthalpy can be derived.

Finally, the constitutive relations are applied to mass and energy conservation equations:

$$S_o + S_g + S_w = 1 \quad (8)$$

$$\sum_i X_{i\beta} = 1, \beta = o, g \quad (9)$$

As solid organic matter pyrolysis, the pore space of shale matrix evolves. The porosity and permeability under different concentration of solid organic substance is expressed as (Liu et al., 2020b):

$$\phi^{t+1} = \frac{C_s^t - C_s^{t+1}}{\rho_s} + \phi^t \quad (10)$$

$$k^{t+1} = k^t \left(\frac{\phi^{t+1}}{\phi^t} \right)^{c_k} \left(\frac{1 - \phi^t}{1 - \phi^{t+1}} \right)^2 \quad (11)$$

where t is time step; ρ_s is the molar density of solid organic matter, mol/m³; c_k is the Carmen-Kozeny coefficient.

2.2 Kinetic reaction model

Solid kerogen pyrolysis and cracking of hydrocarbon take place when shale formation reaches designed temperature. In our model, pseudo component IC₃₇, IC₁₃ and IC₂ are used to represent heavy oil, light oil and hydrocarbon gas, respectively. The chemical kinetic reaction equations and corresponding kinetics parameters are given in Table 1 (Lee et al., 2018a).

Above kinetic reactions are controlled by pyrolysis kinetics parameters (Tissot and Welte, 2013) and can be handled with first order general-package pyrolysis model. The reaction rate is given by (Wang et al., 1984; Li et al., 1995):

$$r_k = K_k \prod_{i,\beta} C_{i\beta}^{v_{i\beta,k}} \prod_s C_s^{v_{s,k}} \quad (12)$$

where $C_{i\beta}$ is the concentration of component i in phase β , mol/m³; K_k is the reaction constant of the k -th reaction, s⁻¹, and is given by Arrhenius law:

$$K_k = A_k \exp\left(-\frac{E_k}{RT}\right) \quad (13)$$

where A_k is the frequency factor of the k -th reaction, s⁻¹; E_k represents the reaction activation energy of the k -th reaction, J/mol; R is the universal gas constant, 8.314 J/(mol·K).

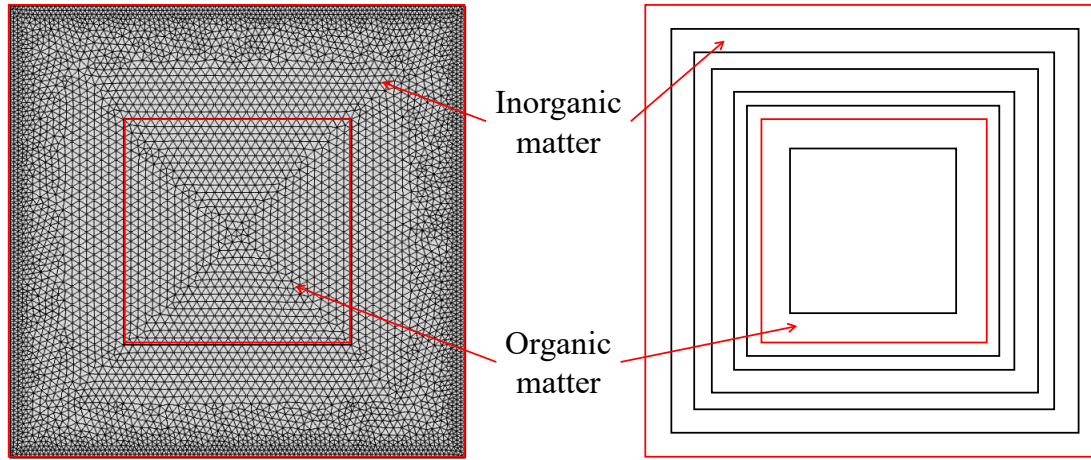
2.3 Solution strategy

Finite volume method is applied to discretize the mass and energy conservation equations. Due to highly nonlinear governing equations, first-order backward finite difference scheme is applied to discretize time. Flux and source terms discretization are carried out fully implicitly. Finally, discretized mass and energy conservation equation can be written into residual form as follows:

$$\left\{ \begin{aligned} R_{\beta,i}^{t+1} &= \sum_{m \in \eta_n} \left[\sum_{\beta} (\rho_{\beta} X_{i\beta} \lambda_{\beta})_{nm+1/2}^{t+1} T_{nm}^{t+1} (\psi_{\beta m}^{t+1} - \psi_{\beta n}^{t+1}) \right] + \left(V \sum_{\beta} \rho_{\beta} X_{i\beta} q_{\beta}^w \right)_n^{t+1} + \left(V \sum_{\beta} \sum_k (v'_{i\beta,k} - v_{i\beta,k}) r_k \right)_n^{t+1} \\ &\quad - \frac{\left\{ V \left[\phi \sum_{\beta} (S_{\beta} \rho_{\beta} X_{i\beta}) \right] \right\}_n^{t+1} - \left\{ V \left[\phi \sum_{\beta} (S_{\beta} \rho_{\beta} X_{i\beta}) \right] \right\}_n^t}{\Delta t} \\ R_w^{t+1} &= \sum_{m \in \eta_n} \left[(\rho_w \lambda_w)_{nm+1/2}^{t+1} T_{nm}^{t+1} (\psi_{wm}^{t+1} - \psi_{wn}^{t+1}) \right] + (V \rho_w q_w)_n^{t+1} - \frac{(V \phi \rho_w S_w)_n^{t+1} - (V \phi \rho_w S_w)_n^t}{\Delta t} \\ R_s^{t+1} &= \left(V \sum_k (v'_{s,k} - v_{s,k}) r_k \right)_n^{t+1} - \frac{(V C_s)_n^{t+1} - (V C_s)_n^t}{\Delta t} \\ R_E^{t+1} &= \sum_{m \in \eta_n} \left[\sum_{\beta} (\rho_{\beta} \lambda_{\beta} H_{\beta})_{nm+1/2}^{t+1} T_{nm}^{t+1} (\psi_{\beta m}^{t+1} - \psi_{\beta n}^{t+1}) \right] + \sum_{m \in \eta_n} \left[\left(\frac{A_{nm} \kappa_{nm+1/2}}{d_n + d_m} \right)^{t+1} (T_m^{t+1} - T_n^{t+1}) \right] + \left(V \sum_{\beta} H_{\beta} \rho_{\beta} q_{\beta}^w \right)_n^{t+1} \\ &\quad + (V q^H)_n^{t+1} - \frac{\left\{ V \left[\phi \sum_{\beta} U_{\beta} \rho_{\beta} S_{\beta} + (1 - \phi) \rho_R U_R \right] \right\}_n^{t+1} - \left\{ V \left[\phi \sum_{\beta} U_{\beta} \rho_{\beta} S_{\beta} + (1 - \phi) \rho_R U_R \right] \right\}_n^t}{\Delta t} \end{aligned} \right. \quad (14)$$

Table 1. Chemical reactions and kinetic reaction parameters during in-situ conversion process.

Number	Reactions	Frequency factor/day	Activation energy/kJ·mol ⁻¹
1	Kerogen(s)→0.0098IC ₃₇ +0.0175IC ₁₃ +0.04002IC ₂ +0.00541CO ₂	3.74×10 ¹²	161.6
2	IC ₃₇ (g)→0.2034IC ₁₃ +2.1153IC ₂	7.95×10 ¹⁶	206.034
3	IC ₃₇ (o)→1.8269IC ₁₃ +0.0402IC ₂	7.95×10 ¹⁶	206.034
4	IC ₁₃ (g)→5.1983IC ₂	5.85×10 ¹⁶	219.328
5	IC ₁₃ (o)→0.5125IC ₂	5.85×10 ¹⁶	219.328

**Fig. 1.** Schematic of computational refined grid (left) and MINC grid (right).

where λ is the mobility, given by $\lambda = k_r/\mu$, mPa⁻¹·s⁻¹; subscript $nm + 1/2$ represents proper average at interface between elements n and m ; η_n denotes all the neighbor grid cells of element n ; T_{nm} is the transmissibility between elements n and m , determined by:

$$T_{nm} = \frac{A_{nm}K_{nm+1/2}}{d_n + d_m} \quad (15)$$

where A_{nm} is the interface area, m²; d^n and d^m represent distance to the interface, m. In this study, the mobility and transmissibility are derived with the upstream-weighting and harmonic mean methods, respectively.

The above conservation equations are solved with Newton-Raphson iteration method, until the convergence criterion is satisfied. The following schemes are given by:

$$\sum_{l=1}^{N_c+3} \frac{\partial R_{l,n}^{j+1}(x_p^{j+1})}{\partial x_l} \delta x_{l,p+1} = -R_{l,n}^{j+1}(x_p^{j+1}) \quad (16)$$

$$x_{p+1}^{j+1} = x_p^{j+1} + \delta x_{p+1} \quad (17)$$

where subscript l denote the l -th primary variable; N_c is the number of components; j is the iteration step; $\delta x_{l,j+1}$ is the increment of primary variables; x represents the vector of primary variables, including reservoir pressure p_o , water saturation S_w and fluid composition z_i ($i = 1, \dots, N_c - 1$).

3. Results analysis

3.1 Model validation

To validate our model in simulating the in-situ conversion process in low-medium maturity shale reservoir, we carried out several numerical cases. Firstly, we validated the multi-continuum model with refined grid simulation results from COMSOL. Sequentially, the thermal-reactive compositional model is verified and more specific description can be found in Wang et al. (2021).

In this section, we build a two-dimension square shaped shale matrix with separated organic and inorganic system. The matrix dimension is 10×10 m², with central 5×5 m² organic region. The boundary pressure is constantly kept at 5 MPa. The porosity of whole shale matrix is 0.08. The initial fluid pressure is 20 MPa and is saturated by single oil phase. The permeability of organic and inorganic shale matrix is 1×10⁻²⁰ m² and 1×10⁻¹⁹ m², respectively. Refined grids result is simulated in COMSOL, taken as the reference. In MINC model, primary grid is divided into 8 nested subgrids. The scheme of multiscale shale matrix and different gridding strategies are shown in Fig. 1. The comparisons of cumulative oil production with two different subdividing strategies are illustrated in Fig. 2. It can be seen that MINC method can obtain the same result as that of refined grids with fewer grid cells. In addition, MINC method is more computationally efficient than refined grids in single continuum model.

3.2 Application of multi-continuum model in low-moderate shale reservoir

In this section, we concentrate on the application of our multi-continuum model in the simulating of in-situ conversion technology. A typical multiscale shale oil reservoir with one production well and hexagon heating wells is established and MINC method is applied to shale matrix grid, as shown in Fig. 3. The numerical model is initialized using parameters from typical shale oil reservoirs, given in Table 2. Kerogen decomposition and hydrocarbon cracking are quite complicate, in which hundreds of reactants and products can be involved. Therefore, components with similar properties are lumped and pseudo components IC₃₇, IC₁₃ and IC₂ are used to represent heavy oil, light oil and hydrocarbon gas, respectively. Thermodynamic properties of these pseudo component are listed in Table 3.

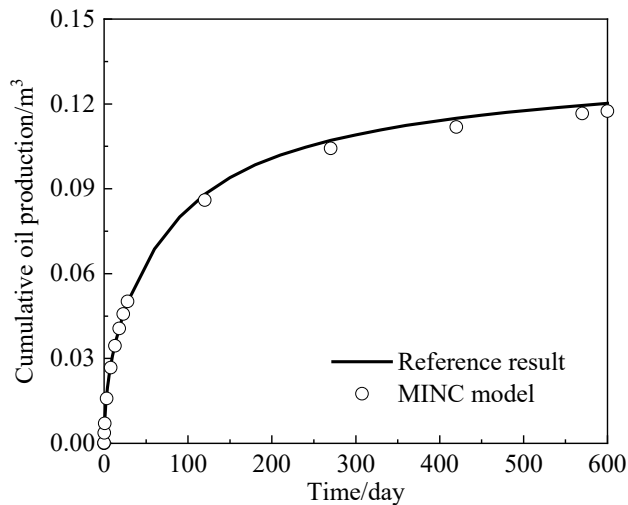


Fig. 2. Comparisons of cumulative oil production from MINC model and reference results.

In order to evaluate the feasibility of in-situ conversion process, the oil and gas cumulative production of artificial conversion and depletion are compared, and the result is shown in Fig. 4. It can be seen that cumulative hydrocarbon production increases dramatically after in-situ conversion. However, in the depletion case, the production rate declines quickly and only limited oil and gas are naturally produced. Due to low thermal maturation of shale, storage space is not developed and retained hydrocarbon is of high viscosity. Therefore, only a few of un-expelled oil and gas can be produced during the short-term depletion and the production rate declines quickly. While during in-situ conversion process, shale formation is heated and a series of chemical kinetic reactions occur, leading to additional artificial oil and gas production.

Table 2. Basic model parameters of shale oil reservoir.

Parameters	Unit	Value
Model dimension	m	30×30×20
Grid number	-	38×38×1
Porosity	-	0.05
Organic matter permeability	m ²	1.5×10 ⁻¹⁹
Inorganic matter permeability	m ²	2×10 ⁻²⁰
Organic volume fraction	-	0.31
Shale density	kg/m ³	2850
Shale heat capacity	J/(kg·K)	1046.7
Shale compressibility	Pa ⁻¹	1×10 ⁻⁹
Initial reservoir pressure	MPa	25
Initial reservoir temperature	K	353.15
Initial water saturation	-	0.1
Well bottom hole pressure	MPa	9.5
Heating temperature	K	600
Simulation time	day	1500

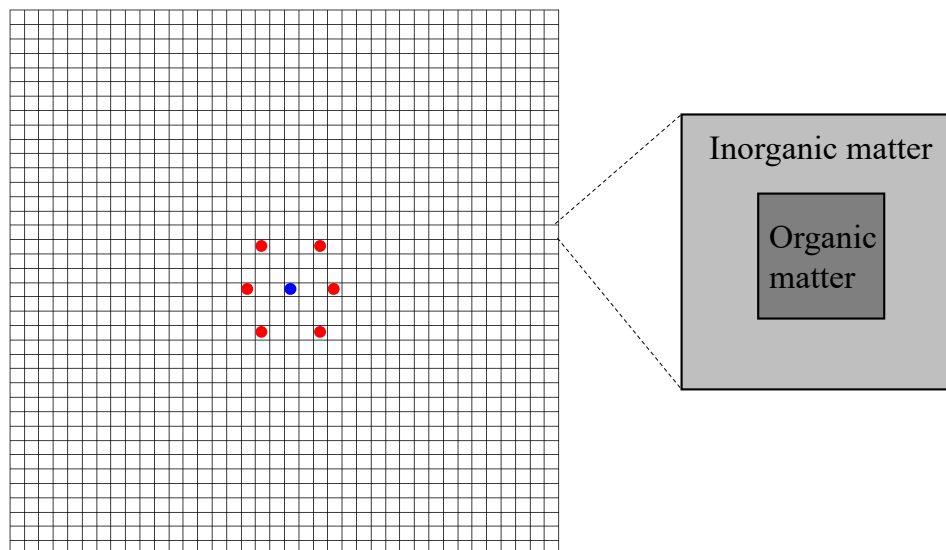
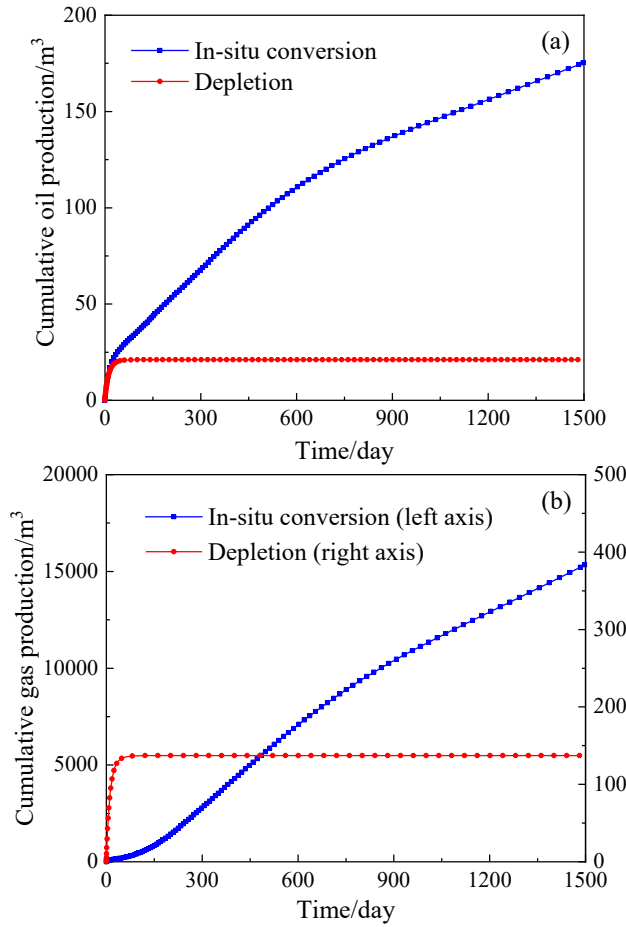


Fig. 3. The schematic diagram of the hexagon heating pattern and computational grids. Blue dot and red dots indicate production well and heating wells, respectively.

Table 3. The calculating parameters for fluid phase behavior.

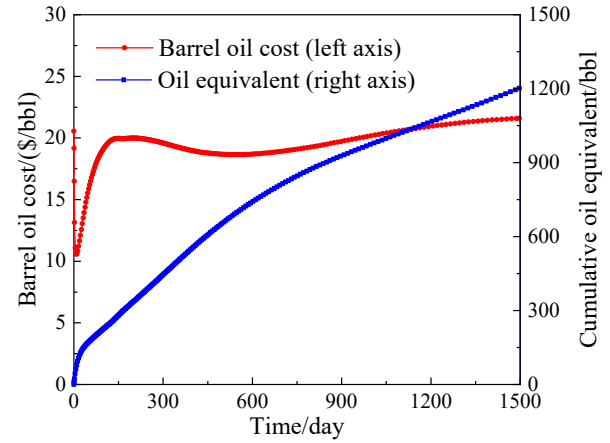
Component	Molecular weight/g·mol ⁻¹	Pc/bar	Tc/K	Acentric factor	Molar fraction/%
CO ₂	44.01	73.80151	304.2	0.225	2.109349
N ₂	28.013	33.9439	126.2	0.039	8.243334
IC ₂	30.07	46.09009	288.7444	0.008	5.273372
IC ₁₃	169.52	24.0503	715.3611	0.365	10.54674
IC ₃₇	465.83	9.3555	962.2833	0.818	73.8272

**Fig. 4.** Comparisons of cumulative (a) oil production and (b) gas production of in-situ conversion and depletion.

In addition, the energy cost of in-situ conversion production should also be considered because large amount of energy is required to heat target shale formation. In this section, cumulative gas production is converted into oil equivalent by regarding 155.12 m³ gas equivalent to 1 barrel of oil and the heat value of 1 barrel of oil is 5.6 MMBtu (Fan et al., 2010). With the calorific value price of natural gas 2.6 \$/MMBtu taken as reference, energy cost per barrel oil can be given by (Tatyana and Eduardo, 2017):

$$cost_{BOE} = \frac{E_{in}}{BOE} \times cost_{gas}/e \quad (18)$$

where $cost_{BOE}$ is energy cost per barrel, \$/bbl; E_{in} is cumulative energy input, MMBtu; BOE is oil equivalent production,

**Fig. 5.** The variation of energy cost per barrel oil with time during 1500 days of in-situ conversion.

bbl; $cost_{gas}$ represents calorific value price of natural gas, \$/MMBtu; e is energy conversion efficiency.

The cost of in-situ conversion during 1500 days heating is illustrated in Fig. 5. As shown in Fig. 5, the energy cost increases quickly at early production and then decreases slightly, finally remains between 18.79 \$/bbl and 21.59 \$/bbl. This is because the energy is injected to formation while limited retained oil and gas can be produced at the early period, leading to cost increment. As shale formation is heated, the decomposition of kerogen and cracking of hydrocarbon take place, providing more artificial hydrocarbon and thus cutting down the energy cost.

3.3 Sensitivity analysis of in-situ conversion process

3.3.1 Effect of heating temperature

During in-situ conversion, several kinetic reactions take place sequentially. And heating temperature has great impact on reaction type and rate. In this section, three numerical experiments are conducted with heating temperature of 600 K, 580 K, 560 K. Other reservoir properties and operation parameters are identical to those in section 3.2, similarly hereinafter. The comparisons of cumulative oil and gas with different heating temperature are shown in Fig. 6. From Fig. 6 it can be seen that hydrocarbon production increases with higher heating temperature. This is because chemical kinetic reaction can be accelerated with higher energy injection rate. Meanwhile, from Eq. (12), the starting temperature of each

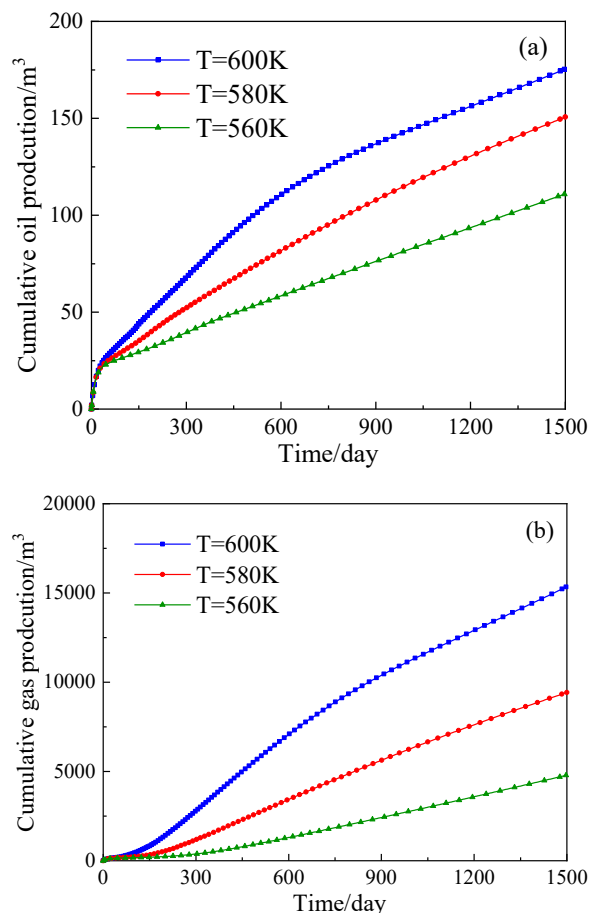


Fig. 6. Comparisons of cumulative (a) oil production and (b) gas production with different heating temperature after 1500 days of in-situ conversion process.

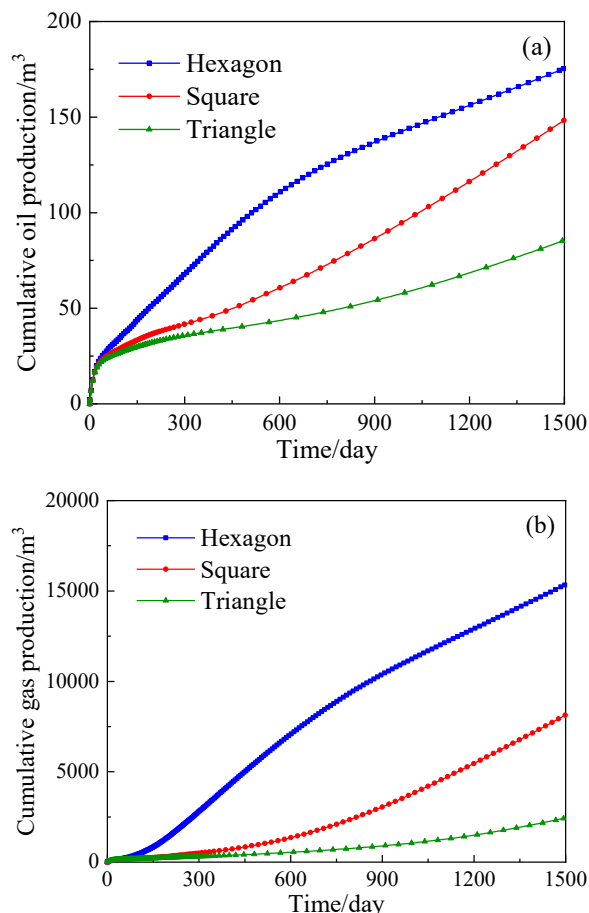


Fig. 8. Comparisons of cumulative (a) oil production and (b) gas production with different heating pattern after 1500 days of in-situ conversion process.

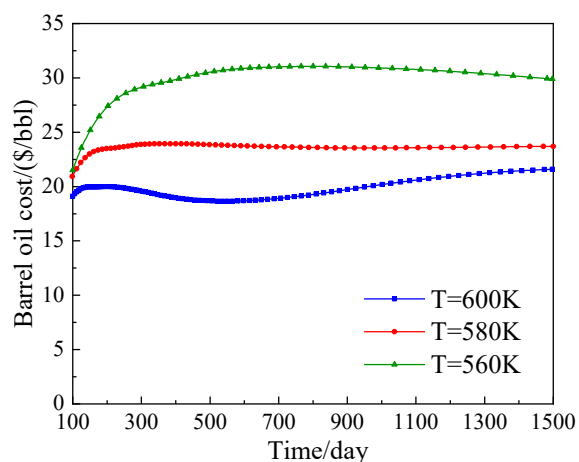


Fig. 7. Comparisons of energy cost per barrel oil with different heating temperature after 1500 days of in-situ conversion.

kinetic reactions can be derived and the required temperature for kerogen decomposition and hydrocarbon cracking is 544 K and 569 K, respectively. Therefore, only kerogen pyrolysis is involved in the 560 K heating temperature. The 560 K heating case has slower gas production rate and finally leads to the lowest hydrocarbon production. The energy cost per barrel oil

during in-situ conversion is given in Fig. 7. It is clear that the energy cost per barrel oil decreases against higher heating temperature. Although more energy is injected with higher heating temperature, more kinetic reactions can take place, providing more mobile oil and gas and thus cutting down the energy cost.

3.3.2 Effect of heating pattern

In actual reservoir development, plenty of heating and production wells should be assigned on the target formation. A typical production unit of in-situ conversion usually contains one production well, surrounded by several heating wells. In our study, we focus on the hydro-thermal coupling mechanism in one typical production unit. In this section, we design hexagon, square and triangle heating pattern and investigate its impact on cumulative production. Fig. 8 shows the comparisons of cumulative production of oil and gas with different heating patterns. It is obvious that hexagon heating pattern can produce more oil and gas than other two cases. In addition, gas production with hexagon heating pattern increases more quickly while triangle heating pattern takes longer time to heat shale formation to designed temperature. Fig. 9 illustrates the energy cost per barrel oil with different heating pattern. It can be seen that hexagon heating pattern has lowest average energy cost while triangle heating pattern has limited economic bene-

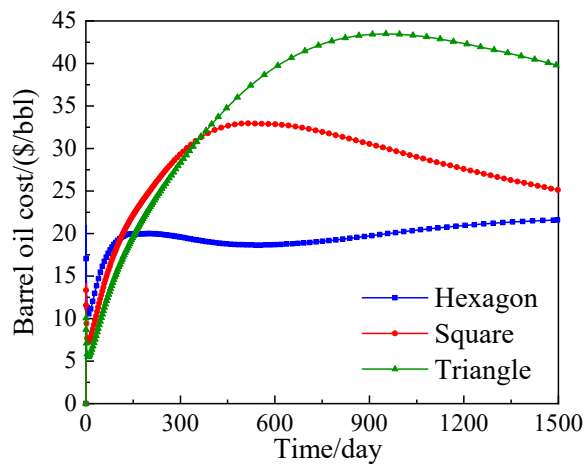


Fig. 9. Comparisons of energy cost per barrel oil with different heating pattern after 1500 days of in-situ conversion.

fit. This is because the heat conduction in shale reservoir is a slow process. Triangle heating pattern is relatively sparse and it takes more time to heat shale formation. Conversely, hexagon heating pattern has highest heating efficiency and lowest energy cost.

4. Conclusions

In this paper, a multi-continuum model considering coupled hydro-thermal process is developed, in which the transient interaction between organic and inorganic system, shale oil upgrading and porosity evolution are incorporated. Several numerical cases are carried out to evaluate the feasibility of in-situ conversion and investigate key influencing factors that affect shale oil production. The conclusions are as follows:

- 1) Due to low storage capacity of primary pore space, depletion is insufficient to obtain economic yield. In-situ conversion technology is feasible in low-medium maturity shale oil reservoir, and can remain high production rate for a long term compared with depletion production. The energy cost per barrel oil basically remains between 18.79 and 21.59 \$/bbl.
- 2) Heating temperature and organic matter content determine reaction rate and type. More kinetic reactions (e.g., hydrocarbon cracking) can be involved with higher heating temperature to further upgrade shale oil.
- 3) Hexagon heating pattern has higher heating efficiency and lower energy cost per barrel oil. Although triangle heating pattern is less expensive to practice, it takes long time to reach desired temperature due to slow heat propagation.

Acknowledgement

The authors would like to appreciate the support of National Natural Science Foundation of China (52034010, 52122402, 52004321), Graduate Innovative Engineering Funding Project (YCX2021036), Natural Science Foundation of Shandong Province, China (ZR2020QE116), China Postdoctoral Science Foundation (2020M682265), Postdoctoral Innovation Fund of Shandong Province (202003016), Fundamental Research Funds for the Central Universities (20CX06025A,

20CX06088A), and Qingdao Postdoctoral Applied Research project (QDYY20190025, QDYY20200083).

Conflict of interest

The authors declare no competing interest.

Open Access This article is distributed under the terms and conditions of the Creative Commons Attribution (CC BY-NC-ND) license, which permits unrestricted use, distribution, and reproduction in any medium, provided the original work is properly cited.

References

- Barenblatt, G. I. Basic concepts in the theory of seepage of homogeneous liquids in fissured rocks. *Journal of Applied Mathematics and Mechanics*, 1960, 24(5): 1286-1303.
- Bi, H., An, C., Chen, X., et al. Investigation into the oil removal from sand using a surface washing agent under different environmental conditions. *Journal of Environmental Management*, 2020, 275: 111232.
- Braun, R. L., Burnham, A. K. Analysis of chemical reaction kinetics using a distribution of activation energies and simpler models. *Energy & Fuels*, 1987, 1(2): 153-161.
- Braun, R. L., Burnham, A. K. Mathematical model of oil generation, degradation, and expulsion. *Energy & Fuels*, 1990, 4(1): 132-146.
- Cheng, S., Huang, P., Wang, K., et al. Comprehensive modeling of multiple transport mechanisms in shale gas reservoir production. *Fuel*, 2020, 277: 118159.
- Egboga, N., Kishore, K., Matthew, T. A feasibility study of thermal stimulation in unconventional shale reservoirs. *Journal of Petroleum Science and Engineering*, 2017, 154: 576-588.
- Fan, W., Sun, H., Yao, J., et al. A new fractal transport model of shale gas reservoirs considering multiple gas transport mechanisms, multi-scale and heterogeneity. *Fractals*, 2018, 26: 1850096.
- Fan, Y., Louis, D., Hamdi, A. Numerical simulation of the in-situ upgrading of oil shale. *SPE Journal*, 2010, 15(2): 368-381.
- Farah, N., Ding, D., Wu, Y., et al. Simulation of fracturing water invasion and its impact on gas production in shale-gas reservoirs. Paper SPE 173264 Presented at ECMOR XIV-14th European conference on the mathematics of oil recovery, Catania, Sicily, 8-11 September, 2014.
- Fowler, T., Harold, J. Oil shale ICP-Colorado field pilots. Paper SPE 121164 Presented at SPE western regional meeting, San Jose, California, 24-26 March, 2009.
- Gao, Z., Fan, Y., Xuan, Q., et al. A review of shale pore structure evolution characteristics with increasing thermal maturities. *Advances in Geo-Energy Research*, 2020, 4(3): 247-259.
- Garipov, T. T., Tomin, P., Rin, R., et al. Unified thermo-compositional-mechanical framework for reservoir simulation. *Computational Geosciences*, 2018, 22: 1039-1057.
- Hazra, K., Lee, K., Economides, C., et al. Comparison of heating methods for in-situ oil shale extraction. Paper cp-342-00038 Presented at IOR 2013-17th European Symposium on Improved Oil Recovery, St. Petersburg, Russia, 16-18 April, 2013.

- Jiang, J., Rami, M. A multimechanistic multicontinuum model for simulating shale gas reservoir with complex fractured system. *Fuel*, 2015, 161: 333-344.
- Kibodeaux, K. Evolution of porosity, permeability, and fluid saturations during thermal conversion of oil shale. Paper SPE 170733 Presented at SPE annual technical conference and exhibition, Amsterdam, The Netherlands, 27-29 October, 2014.
- Lee, K., George, J., Christine, A. A comprehensive simulation model of kerogen pyrolysis for the in-situ upgrading of oil shales. *SPE Journal*, 2016, 21: 1612-1630.
- Lee, K., Stefan, F., George, J. Analyzing the impact of reaction models on the production of hydrocarbons from thermally upgraded oil shales. *Journal of Petroleum Science and Engineering*, 2018a, 168: 448-464.
- Lee, K., Stefan, F., George, J. Estimating the reaction parameters of oil shale pyrolysis and oil shale grade using temperature transient analysis and inverse modeling. *Journal of Petroleum Science and Engineering*, 2018b, 165: 765-776.
- Li, S., Wang, J., Wu, Z., et al. Study on reaction-kinetics of oil-shale and source-rock. *Oil Shale*, 1995, 12: 15-30.
- Liu, L., Huang, Z., Yao, J., et al. An efficient hybrid model for 3D complex fractured vuggy reservoir simulation. *SPE Journal*, 2020a, 25(2): 907-924.
- Liu, L., Huang, Z., Yao, J., et al. Simulating two-phase flow and geomechanical deformation in fractured karst reservoirs based on a coupled hydro-mechanical model. *International Journal of Rock Mechanics and Mining Sciences*, 2021a, 137: 104543.
- Liu, L., Liu, Y., Yao, J., et al. Efficient coupled multiphase-flow and geomechanics modeling of well performance and stress evolution in shale-gas reservoirs considering dynamic fracture properties. *SPE Journal*, 2020b, 25(3): 1523-1542.
- Liu, P., Li, J., Sun, S., et al. Numerical investigation of carbonate acidizing with gelled acid using a coupled thermal-hydrologic-chemical model. *International Journal of Thermal Sciences*, 2021b, 160: 106700.
- Naraghi, M., Farzam, J. A stochastic permeability model for the shale-gas systems. *International Journal of Coal Geology*, 2015, 140: 111-124.
- Oja, V., Eric, M. Oil shale processing, chemistry, and technology, in *Fossil Energy*, edit by R. Malhotra, Springer, New York, pp. 47-83, 2020.
- Tatyana, P., Eduardo, G. Rigorous integrated evolutionary workflow for optimal exploitation of unconventional gas assets. *International Journal of Energy Optimization and Engineering*, 2017, 6(1): 101-121.
- Tissot, B. P., Welte, D. H. *Petroleum Formation and Occurrence*. Berlin, German, Springer-Verlag Berlin Heidelberg, 2013.
- Wang, J., Qian, J., Wu, L. Kinetic study on hydrocarbon forming pyrolysis of Fushun and Maoming oil shales. Paper CONF-840415 Presented at National Meeting of the American Chemical Society, St. Louis, MO, 8 April, 1984.
- Wang, S., Feng, Q., Farzam, J., et al. Oil adsorption in shale nanopores and its effect on recoverable oil-in-place. *International Journal of Coal Geology*, 2015, 147: 9-24.
- Wang, Z., Yao, J., Sun, H., et al. Coupled thermal-reactive flow simulation of in-Situ conversion in 3D low-mid maturity shale oil reservoir. Paper ARMA 21-2118 Presented at 55th US Rock Mechanics/Geomechanics Symposium, Houston, Texas, 20-23 June, 2021.
- Warren, J., Root, P. The behavior of naturally fractured reservoirs. *SPE Journal*, 1963, 3(3): 245-255.
- Wu, Y., Pruess, K. A multiple-porosity method for simulation of naturally fractured petroleum reservoirs. *SPE Reservoir Engineering*, 1988, 3(1): 327-336.
- Yang, Y., Liu, X., Hang, H., et al. A review and research on comprehensive characterization of microscopic shale gas reservoir space. *China Geology*, 2019a, 2(4): 541-556.
- Yang, Z., Zou, C., Wu, S., et al. Formation, distribution and resource potential of the "sweet areas (sections)" of continental shale oil in China. *Marine and Petroleum Geology*, 2019b, 102: 48-60.
- Yan, X., Huang, Z., Yao, J., et al. An efficient numerical hybrid model for multiphase flow in deformable fractured-shale reservoirs. *SPE Journal*, 2018, 23: 1412-1437.
- Zhang, M., Yao, J., Sun, H., et al. Triple-continuum modeling of shale gas reservoirs considering the effect of kerogen. *Journal of Natural Gas Science and Engineering*, 2015, 24: 252-263.
- Zhao, W., Hu, S., Hou, L., et al. Types and resource potential of continental shale oil in China and its boundary with tight oil. *Petroleum Exploration and Development*, 2020, 47(1): 1-11.
- Zhu, G., Li, A. Interfacial dynamics with soluble surfactants: A phase-field two-phase flow model with variable densities. *Advances in Geo-Energy Research*, 2020, 4(1): 86-98.